Available online at www.sciencedirect.com
ScienceDirect
Trans. Nonferrous Met. Soc. China 32(2022) 503−512
Transactions of Nonferrous Metals Society of China
www.tnmsc.cn

Microstructure and mechanical properties of Ti−Nb−Fe−Zr alloys with high strength and low elastic modulus

Qiang LI[1], Qi HUANG[1], Jun-jie LI[2], Qian-feng HE[1], Masaaki NAKAI[3], Ke ZHANG[4], Mitsuo NIINOMI[1,5,6,7], Kenta YAMANAKA[5], Akihiko CHIBA[5], Takayoshi NAKANO[6]

1. School of Mechanical Engineering, University of Shanghai for Science and Technology, Shanghai 200093, China;
2. CAS Key Laboratory of Functional Materials and Devices for Special Environments, Xinjiang Technical Institute of Physics & Chemistry, CAS, Urumqi 830011, China;
3. Division of Mechanical Engineering, Faculty of Science and Engineering, Kindai University, 3-4-1 Kowakae, Higashiosaka, Osaka 577-8502, Japan;
4. School of Materials Science and Engineering, University of Shanghai for Science and Technology, Shanghai 200093, China;
5. Institute for Materials Research, Tohoku University, 2-1-1 Katahira, Aoba-ku, Sendai 980-8577, Japan;
6. Division of Materials and Manufacturing Science, Graduate School of Engineering, Osaka University, 2-1 Yamada-Oka, Suita, Osaka 565-0871, Japan;
7. Department of Materials Science and Engineering, Graduate School of Science and Technology, Meijo University, 1-501 Shiogamaguchi, Tempaku-ku, Nagoya 468-8502, Japan

Received 26 January 2021; accepted 20 October 2021

Abstract: Zr was added to Ti−Nb−Fe alloys to develop low elastic modulus and high strength β-Ti alloys for biomedical applications. Ingots of Ti−12Nb−2Fe−(2, 4, 6, 8, 10)Zr (at.%) were prepared by arc melting and then subjected to homogenization, cold rolling, and solution treatments. The phases and microstructures of the alloys were analyzed by optical microscopy, X-ray diffraction, and transmission electron microscopy. The mechanical properties were measured by tensile tests. The results indicate that Zr and Fe cause a remarkable solid-solution strengthening effect on the alloys; thus, all the alloys show yield and ultimate tensile strengths higher than 510 MPa and 730 MPa, respectively. Zr plays a weak role in the deformation mechanism. Further, twinning occurs in all the deformed alloys and is beneficial to both strength and plasticity. Ti−12Nb−2Fe−(8, 10)Zr alloys with metastable β phases show low elastic modulus, high tensile strength, and good plasticity and are suitable candidate materials for biomedical implants.
Key words: biomedical Ti alloy; mechanical properties; solid-solution strengthening; work hardening; twinning-induced plasticity

1 Introduction

Ti and Ti alloys have been widely used as biomedical implants owing to their good comprehensive mechanical properties and corrosion resistance, and excellent biocompatibility [1,2]. However, the health problems arising from the long-term implantation of commercial pure Ti (CP-Ti) and Ti−6Al−4V extro-low interstitial (wt.%) have caused public concern, because these materials show much higher elastic modulus (~110 GPa) than human bones (10−30 GPa), which leads to the “stress shielding” effect [3]. Moreover, the release of V and Al during long-term implantation may cause some health problems [4−7].

Corresponding author: Qiang LI, E-mail: jxli@tju.edu.cn, liqiang@usst.edu.cn; Mitsuo NIINOMI, E-mail: niinomi@imr.tohoku.ac.jp
DOI: 10.1016/S1003-6326(22)65811-4

By contrast, β-type Ti alloys composed of highly biocompatible elements, such as Nb, Ta, and Zr, usually show low elastic modulus. Thus, they have attracted extensive attention and are viewed as good candidates for hard tissue replacement [8,9].

Some β-stabilizing elements, including Nb, Mo, and Ta, are usually added to Ti alloys to obtain the β phase at room temperature [2,10,11]. Neutral elements, such as Zr and Sn, are also added to slightly change the β stability and enhance the strength [2,12,13]. Among the newly developed β-type Ti alloys, Ti−Nb-based alloys, such as Ti−29Nb−13Ta−4.6Zr (wt.%) [14], Ti−24Nb−4Zr−8Sn (wt.%) [13], Ti−13Nb−13Zr (wt.%) [15], Ti−35Nb−7Zr−5Ta (wt.%) [16], and Ti−24Nb−2Zr (at.%; herein, the chemical compositions of alloys are expressed in at.% unless indicated otherwise), usually show low elastic modulus [17]. Fe is a strong β-stabilizing element, and its melting point is lower than that of Nb. Moreover, the price of Fe is lower than those of Nb, Mo, and Ta; therefore, Fe is added to reduce the cost of Ti alloys [18]. However, the excessive addition of Fe results in the formation of an intermetallic compound, thereby causing the embrittlement of the alloys [18,19]. In the previous study, 2 at.% Fe (around 2 wt.%) was added to Ti−Nb alloys, and Ti−(14, 16, 18, 20, 22, 24)Nb−2Fe alloys were prepared and studied [20]. The results indicate that Fe causes a noticeable solid-solution strengthening effect and the Ti−20Nb−2Fe and Ti−22Nb−2Fe alloys exhibit low elastic modulus and suitable plasticity. Zr is a neutral element and is usually viewed as a weak β-stabilizing element for Ti alloys, because it can decrease the martensite start temperature (M_s), which is similar to Nb [10,21]. It also provides a solid-solution strengthening effect and reduces the elastic modulus of the alloys [22]. To reduce the amount of Nb in Ti−20Nb−2Fe and Ti−22Nb−2Fe and improve the mechanical properties, Zr is used to partly replace Nb in Ti−Nb−Fe alloys; thus, Ti−12Nb−2Fe−(2, 4, 6, 8, 10)Zr alloys were prepared and investigated in this study. It is expected that the addition of Zr can slightly adjust the phase stability of the alloys and provide a solid-solution strengthening effect, consequently, new alloys with high strength and low elastic modulus suitable for biomedical implantation will be obtained.

2 Experimental

Ingots of Ti−12Nb−2Fe−(2, 4, 6, 8, 10)Zr were prepared using pure Ti (99.999 wt.%), Nb (99.95 wt.%), Fe (99.95 wt.%), and Zr (99.95 wt.%) by non-consumable arc-melting in a water-sealed copper crucible under a high-purity Ar atmosphere. The ingots were homogenized at 1273 K for 10 h followed by water quenching. After removing the oxide layer, the ingots were cold-rolled at room temperature to a total reduction rate of approximately 83% without intermediate annealing. Sheets with a thickness of 1.6 mm were obtained and then cut into specimens using wire electrical discharge machining. The specimens for the following measurements were solution-treated at 1073 K for 1 h and then water-quenched.

The specimens for the microstructural observations were mechanically ground, mirror-polished, etched in 5 vol.% HF solution, and observed by an optical microscope. X-ray diffraction (XRD) measurement was performed to determine the phase constitutions using a Bruker D8 X-ray diffractometer with Cu K_{α_1} radiation at a voltage of 40 kV and a current of 40 mA. Specimens with the gauge section of 12 mm × 3 mm × 1.5 mm were subjected to tensile tests at room temperature using an universal material testing machine at a cross-head speed of 8.33×10^{-6} m/s. A strain gauge was fixed to the specimens to ensure the accuracy of the strain measurement during the tensile test. The elastic modulus was measured by the free resonance vibration method using the specimens with sizes of 40 mm × 10 mm × 1.5 mm (the details are presented in Refs. [23,24]). The microstructures of the specimens after the solution treatment and tensile tests were further analyzed using transmission electron microscopy (TEM) at a voltage of 200 kV.

3 Results

3.1 Phases and microstructures

The diffraction peak corresponding to the Ti−Fe intermetallic compound is not detected in the XRD patterns of Ti−12Nb−2Fe−(2, 4, 6, 8, 10)Zr after solution treatment (Fig. 1). A weak diffraction peak corresponding to α'' phase is observed in the

pattern of Ti−12Nb−2Fe−6Zr (Fig. 1(c)). Other alloys exhibit single β phases according to the XRD patterns (Figs. 1(a), (b), (d), (e)). The equiaxed β grains are observed in all the Ti−12Nb−2Fe−(2, 4, 6, 8, 10)Zr alloys as typically shown in Fig. 2. The α'' and ω phases are hardly observed by optical microscopy owing to the small size of the phases.

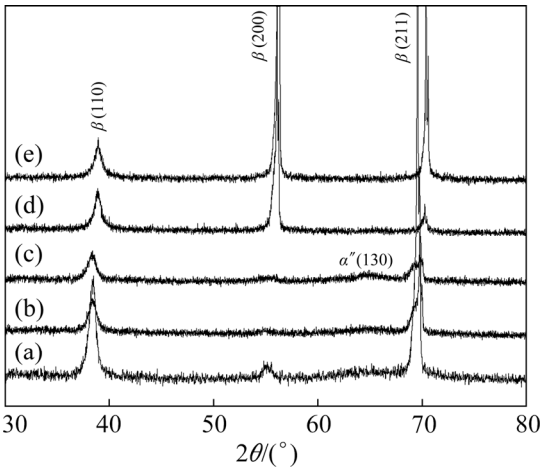

Fig. 1 XRD patterns of Ti−12Nb−2Fe−(2, 4, 6, 8, 10)Zr after solution treatment: (a) Ti−12Nb−2Fe−2Zr; (b) Ti−12Nb−2Fe−4Zr; (c) Ti−12Nb−2Fe−6Zr; (d) Ti−12Nb−2Fe−8Zr; (e) Ti−12Nb−2Fe−10Zr

TEM measurement was performed to further observe the changes in the phases with the increase in Zr content. According to the selected-area electron diffraction (SAED) pattern (insert in Fig. 3(a)), Ti−12Nb−2Fe−2Zr consists of ω and β phases. The nano-sized ω particles can be observed in the dark field (Fig. 3(b)). The SAED spots of α'' phase are found in Ti−12Nb−2Fe−6Zr (insert in Fig. 4(a)), and some small bulk α'' phases can be observed in the dark field (Fig. 4(b)). The SAED pattern (Fig. 5) indicates that Ti−12Nb−2Fe−8Zr consists of a single β phase.

The XRD patterns and TEM results indicate that the phases in the Ti−12Nb−2Fe−(2, 4, 6, 8, 10)Zr alloys change from $\beta+\omega$ phases to $\beta+\alpha''$ phases and then to a single β phase with the increase in Zr content. The structural stability of β-Ti alloys is usually evaluated by the Mo equivalent (Mo_{eq}). WANG et al [25] have developed a formula for calculating $(Mo_{eq})_Q$ by taking some neutral elements, such as Zr and Sn, into consideration. The $(Mo_{eq})_Q$ in at.% (this is the same meaning as $(Mo_{eq})_Q$ in at.% from Ref. [25]), average bonding order ($\overline{B}_o$), and average d-orbital

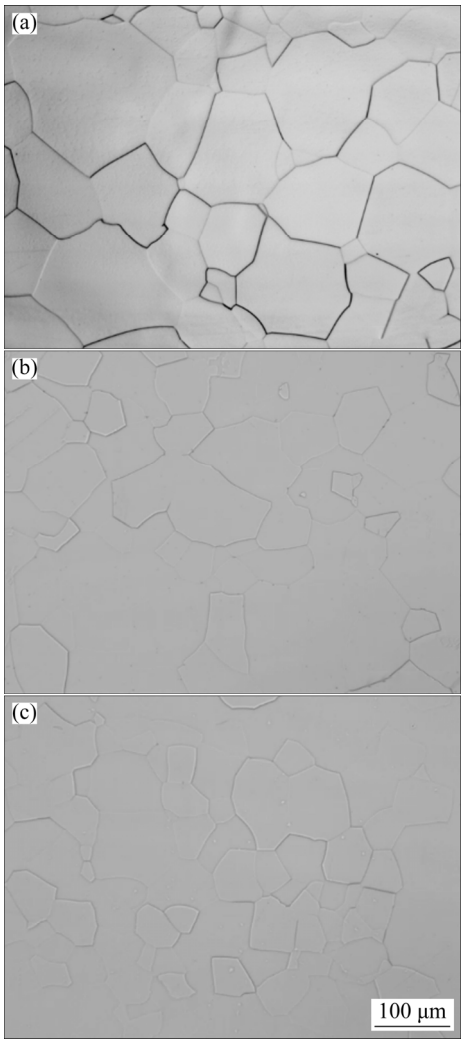

Fig. 2 Optical microstructures of Ti−12Nb−2Fe−2Zr (a), Ti−12Nb−2Fe−6Zr (b), and Ti−12Nb−2Fe−8Zr (c) after solution treatment

energy level ($\overline{M}_d$) values of the alloys are calculated and listed in Table 1 using the formula in Refs. [25,26]. Notably, $(Mo_{eq})_Q$ increases from 5.90 at.% to 8.62 at.% when the Zr content is increased from 2 at.% to 10 at.%. Moreover, both the $\overline{B}_o$ and $\overline{M}_d$ values of the alloys increase with the increase in Zr content. The changes in $(Mo_{eq})_Q$, $\overline{B}_o$, and $\overline{M}_d$ all indicate that the β stability increases owing to the Zr addition in Ti−12Nb−2Fe−(2, 4, 6, 8, 10)Zr. Additionally, the α'' martensite transformation can be suppressed with a further increase in the Zr content because Zr can decrease the M_s point of the alloy [10,21]. This explains why the phase constitution changes from $\beta+\omega$ phases to $\beta+\alpha''$ phases and then to single β phase. Therefore, Ti−12Nb−2Fe−(8, 10)Zr alloys consist of single β phase.

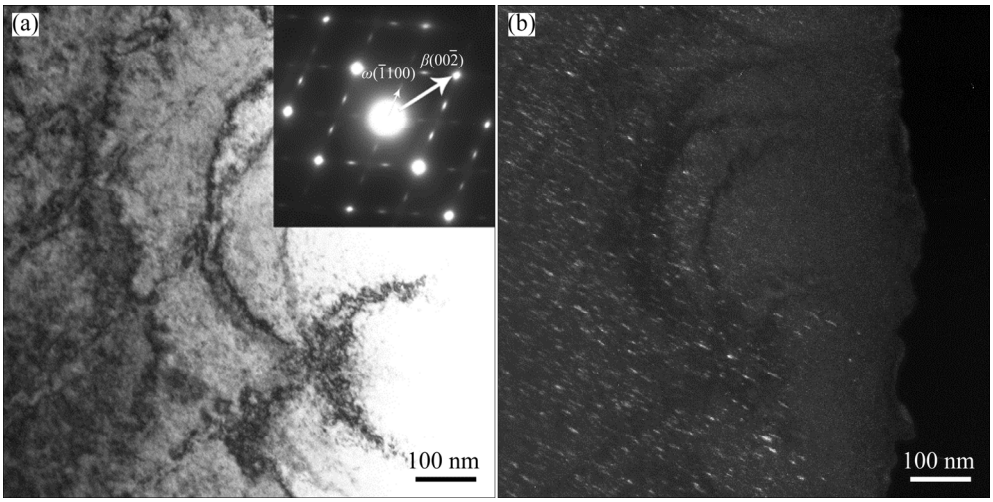

Fig. 3 TEM images of Ti−12Nb−2Fe−2Zr after solution treatment: (a) Bright-field image with SAED pattern; (b) Dark-field image (Beam direction parallel to $[011]_{\beta}$)

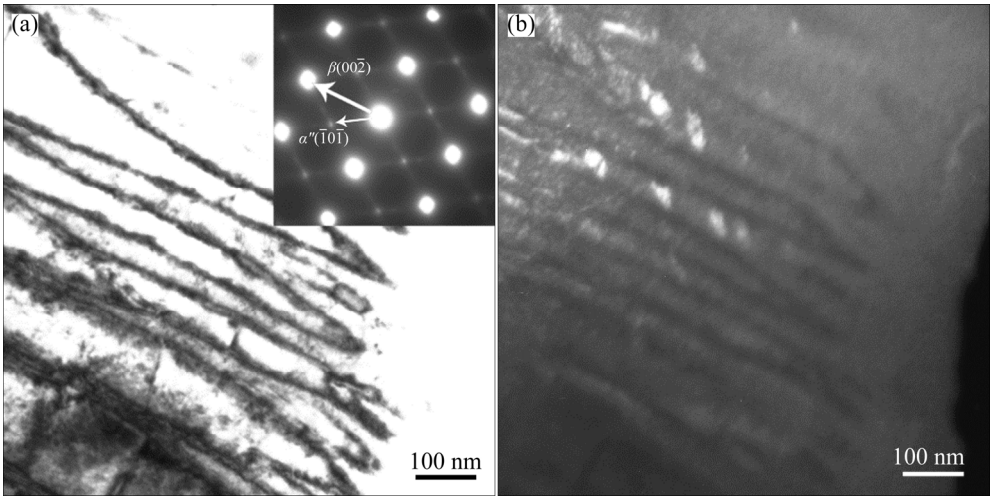

Fig. 4 TEM images of Ti−12Nb−2Fe−6Zr after solution treatment: (a) Bright-field image with SAED pattern; (b) Dark-field image (Beam direction parallel to $[011]_{\beta}$)

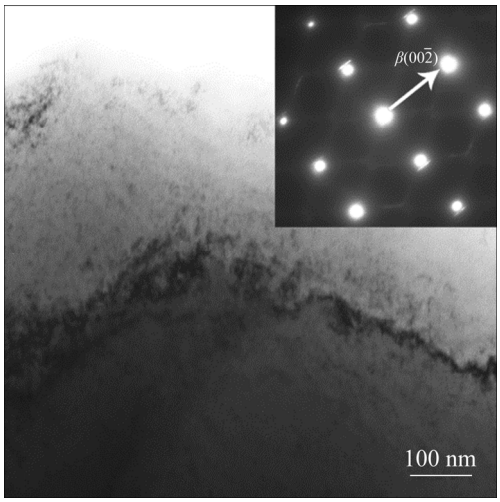

Fig. 5 TEM bright-field image with SAED pattern of Ti−12Nb−2Fe−8Zr after solution treatment (Beam direction parallel to $[011]_{\beta}$)

3.2 Deformation behaviour

According to the true tensile stress–strain curves of the Ti−12Nb−2Fe−(2, 4, 6, 8, 10)Zr alloys after solution treatment (Fig. 6), all the alloys exhibit similar deformation modes during the tensile process, including elastic deformation, plastic deformation, necking, and fracture. Although the double-yield phenomenon is not observed in the curves, a nonlinear deformation between elastic deformation and plastic deformation is observed.

For the specimens obtained after the tensile tests, changes in the phase are not observed from the XRD patterns, but many deformation bands are observed by optical microscopy. Two typical microstructures are found in the deformed alloys.

Table 1 $(Mo_{eq})_Q$, $\overline{B}_o$, and $\overline{M}_d$ for Ti−12Nb−2Fe−(2, 4, 6, 8, 10)Zr alloys

Alloy	$(Mo_{eq})_Q$/at.%	$\overline{B}_o$	$\overline{M}_d$/eV
Ti−12Nb−2Fe−2Zr	5.90	2.830	2.424
Ti−12Nb−2Fe−4Zr	6.58	2.836	2.434
Ti−12Nb−2Fe−6Zr	7.26	2.842	2.444
Ti−12Nb−2Fe−8Zr	7.94	2.848	2.454
Ti−12Nb−2Fe−10Zr	8.62	2.854	2.463

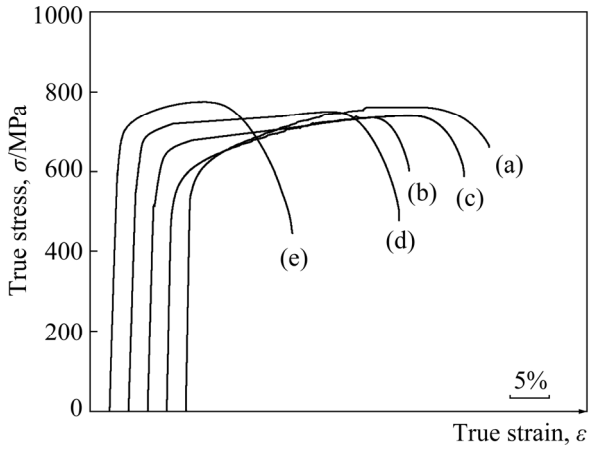

Fig. 6 Tensile true stress–strain curves of Ti−12Nb−2Fe−(2, 4, 6, 8, 10)Zr after solution treatment: (a) Ti−12Nb−2Fe−2Zr; (b) Ti−12Nb−2Fe−4Zr; (c) Ti−12Nb−2Fe−6Zr; (d) Ti−12Nb−2Fe−8Zr; (e) Ti−12Nb−2Fe−10Zr

For Ti−12Nb−2Fe−(2, 4)Zr, many thin interlaced deformation bands appear in the β grains, as typically shown in Fig. 7(a). By contrast, the bands are thicker and almost parallel to each other in the β grains of Ti−12Nb−2Fe−(6, 8, 10)Zr, as typically shown in Fig. 7(b). Two bands with the widths of approximately 200 nm are found in the TEM bright-field image of Ti−12Nb−2Fe−2Zr (Fig. 8(a)), and a band with the width of approximately 2.5 μm is observed in Ti−12Nb−2Fe−8Zr (Fig. 8(c)). Two types of bands are both $\{332\}_\beta\langle 113\rangle_\beta$ twinning based on the SAED patterns (Figs. 8(b) and (d)) obtained at the boundaries. The $\{332\}_\beta\langle 113\rangle_\beta$ twinning in β-Ti alloys is a deformation mechanism of the β phase or a reversion of parent $\{130\}_{\alpha''}\langle 310\rangle_{\alpha''}$ twinning in the stress-induced α'' martensite [27]. As the double-yield phenomenon does not appear during tension and the residual α'' martensite is hardly observed in the alloys, the twinning observed in this study is judged to be the deformation mechanism of the β phase. The size of the bands in Ti−12Nb−2Fe−2Zr is much smaller than that in Ti−12Nb−2Fe−8Zr, which is agreed with the optical microstructures, because the ω phase can hinder large shear deformation and confine the twinning to a smaller scale. The appearance of twinning in the deformed specimens indicates that the β phases in Ti−12Nb−2Fe−(2, 4, 6, 8, 10)Zr are all metastable.

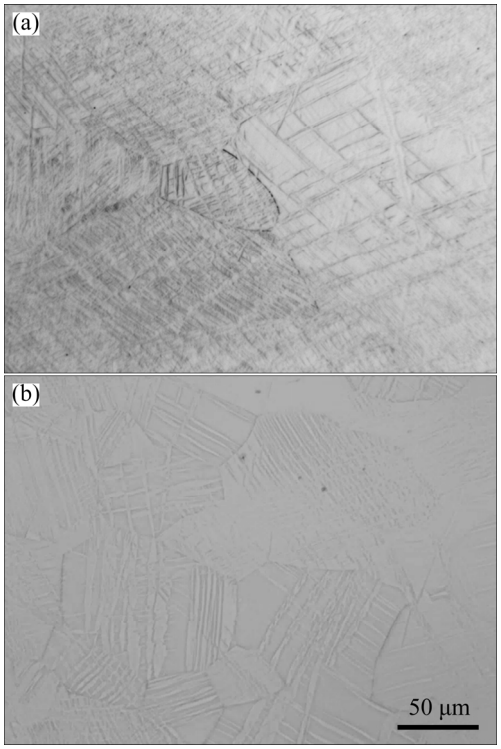

Fig. 7 Optical microstructures of Ti−12Nb−2Fe−2Zr (a) and Ti−12Nb−2Fe−8Zr (b) after tensile tests

The stress of all the alloys increases with increasing applied strain during the plastic deformation stage, indicating that obvious work hardening occurs in all the alloys. The work hardening can be attributed to the strengthening effect during tension. The work hardening ability, which is reflected by the hardening index, is different for each of the Ti−12Nb−2Fe−(2, 4, 6, 8, 10)Zr alloys. The Hollomon equation gives the relationship between true stress and true stain for plastic deformation:

$$\sigma_T = K\varepsilon_T^n$$

where σ_T is the true stress, K is the strength coefficient, ε_T is the true strain, and n is the strain hardening exponent [28,29]. The n values of the Ti−12Nb−2Fe−(2, 4, 6, 8, 10)Zr alloys are calculated to be 0.101, 0.100, 0.050, 0.048, and 0.054, respectively, using the data corresponding to 5%−10%

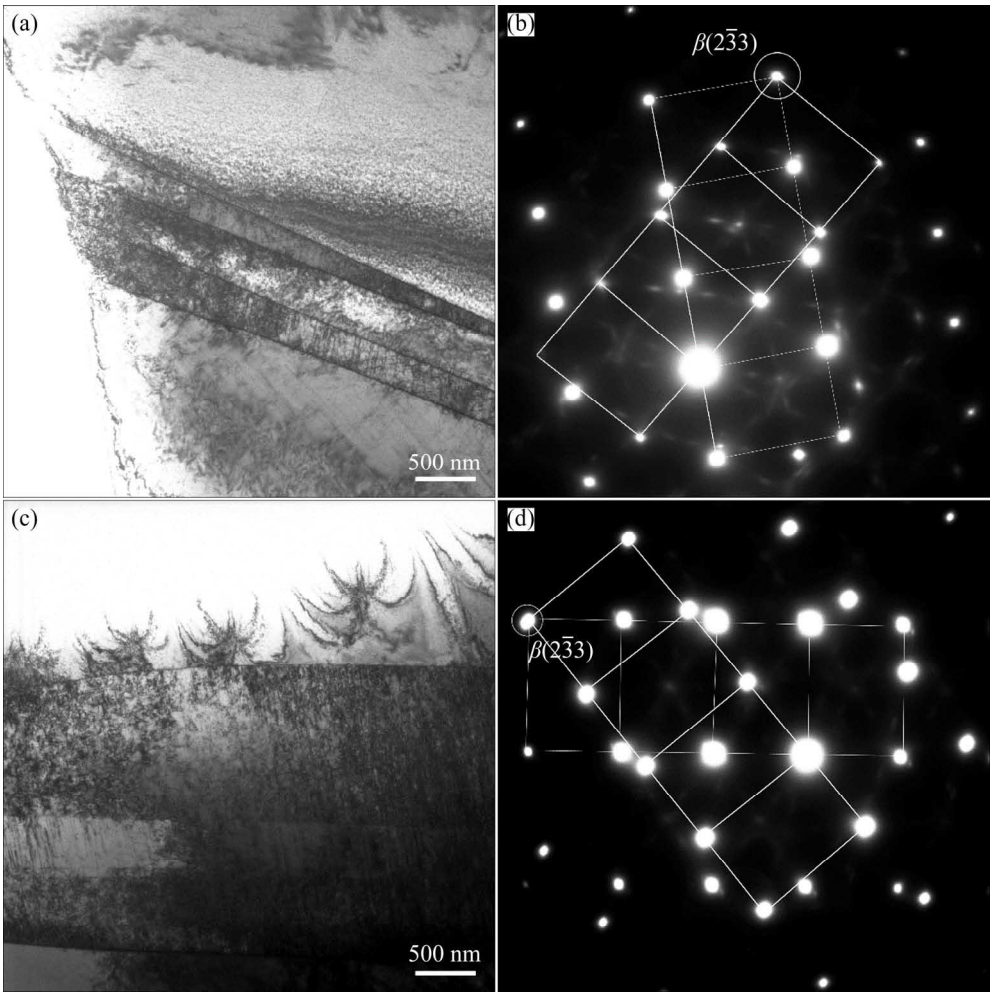

Fig. 8 TEM images obtained from Ti−12Nb−2Fe−2Zr (a, b) and Ti−12Nb−2Fe−8Zr (c, d) after tensile tests: (a, c) Bright-field images; (b, d) SAED patterns (Beam direction parallel to $[011]_{\beta}$)

true strain in Fig. 6. In Ti−12Nb−2Fe−(2, 4)Zr, highly interlaced twinning occurs during tension. Thus, the movement of dislocations is reduced, and the applied stress is continuously increased until necking. Notably, Ti−12Nb−2Fe− 2Zr shows the greatest n value because the ω phase prevents the long-distance movement of dislocations. In Ti−12Nb−2Fe−(6, 8, 10)Zr, ω phase disappears and only parallel twinning exists; consequently, the hardening index values decrease to be around 0.05.

3.3 Mechanical properties

The elastic modulus (E) measured by the free resonance vibration method, 0.2% proof stress ($\sigma_{0.2}$), ultimate tensile strength (σ_b), and elongation (ε) calculated using the stress–strain curves obtained from the tensile tests are shown in Fig. 9. With the increase in Zr content, both σ_b and $\sigma_{0.2}$ show the same trend; namely, they firstly decrease and then increase. The changes in $\sigma_{0.2}$ and σ_b are mainly attributed to the precipitation strengthening caused by ω phase and solid-solution strengthening caused by Zr. Ti−12Nb−2Fe−2Zr shows a $\sigma_{0.2}$ of 548 MPa and a σ_b of 758 MPa owing to the precipitation strengthening of ω phase. With increasing Zr content, the amount of ω phase decreases and even disappears; consequently, the precipitation strengthening effect becomes weak. Meanwhile, the solid-solution strengthening of Zr is gradually enhanced. The strength reduction caused by the disappearance of precipitation strengthening can be partly offset by solid-solution strengthening; thus, the strength only slightly decreases. Ti−12Nb−2Fe−6Zr shows the lowest $\sigma_{0.2}$ and σ_b, which are around 510 and 730 MPa, respectively. When the Zr content is further increased, solid-solution strengthening become obvious; thus, the strength increases gradually in Ti−12Nb−2Fe−(8, 10)Zr.

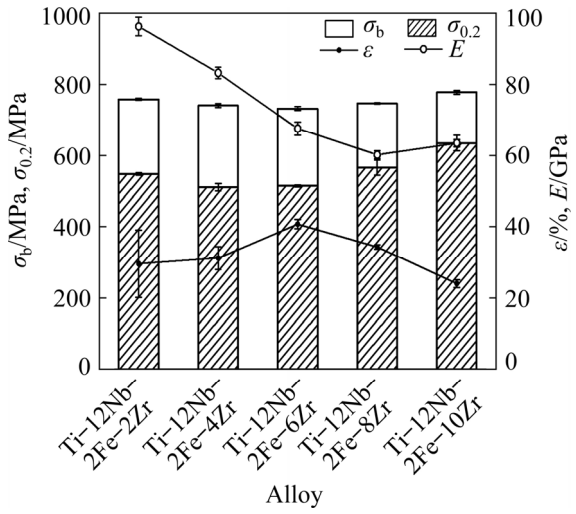

Fig. 9 Elastic modulus (E) measured by free resonance vibration method and 0.2% proof stress ($\sigma_{0.2}$), ultimate tensile strength (σ_b), and elongation (ε) of Ti−12Nb−2Fe−(2, 4, 6, 8, 10)Zr measured by tensile tests

Ti−12Nb−2Fe−10Zr shows the highest $\sigma_{0.2}$ of 635 MPa and the highest σ_b of 778 MPa.

It is widely accepted that both precipitation strengthening and solid-solution strengthening increase the strength but decrease the plasticity. Therefore, with the increase in Zr content, the elongation firstly increases and then decreases, in contrast with the change in strength. Among the Ti−12Nb−2Fe−(2, 4, 6, 8, 10)Zr alloys, Ti−12Nb−2Fe−6Zr exhibits the highest elongation of 40%, and Ti−12Nb−2Fe−10Zr shows the lowest elongation of 24%. Although the strength of these alloys is higher than that of other alloys, the alloys also show good plasticity, mainly owing to the occurrence of twinning, which can cause twinning-induced plasticity (TWIP) [30,31].

The order of the elastic modulus of each phase in Ti alloys is usually $\omega > \alpha > \alpha' > \alpha'' > \beta$ [32,33]. The elastic modulus of an alloy is the weighted average of the elastic modulus of each phase according to its volume fraction. Ti−12Nb−2Fe−2Zr, with ω phase precipitation, shows the highest elastic modulus of 96 GPa. The decrease in elastic modulus is attributed to the changes in the phase composition because the ω and α'' phases are suppressed by Zr addition. Ti−12Nb−2Fe−8Zr shows the lowest elastic modulus of 61 GPa owing to the single metastable β phase. As the Zr content is further increased to 10%, the elastic modulus slightly increases to 63 GPa.

4 Discussion

The oxygen content in Ti alloys is an important factor that influences the mechanical properties and phase composition. High strength and high plasticity can be obtained in Ti−Nb−Ta−Zr−O alloys owing to the Zr−O atom clusters [34]. However, additional oxygen was not added to the studied alloys. Based on infrared absorption, the oxygen content in the studied alloys ranges from 0.07 to 0.09 wt.%, which is a common range for Ti alloys prepared by arc melting [35,36]. Therefore, the β phase stability, deformation mechanism, and mechanical properties are hardly influenced by oxygen content.

Similar to Nb, Zr is reported to stabilize β phase, because it can suppress the ω and α'' transformations during quenching and inhibit the stress-induced α'' martensitic transformation (SIMT) and twinning during deformation [10,17,21]. In Ti−(14−24)Nb−2Fe, twinning is inhibited by adding Nb and is not observed in the deformed Ti−20Nb−2Fe alloy [20]. Similarly, twinning gradually decreases in the deformed Ti−24Nb−(0, 2, 4)Zr and Ti−29Nb−2Cr−(4, 7, 10, 13)Zr (wt.%) alloys with the increase in Zr content [17,37]. By constant, twinning is observed in all the deformed Ti−12Nb−2Fe−(2, 4, 6, 8, 10)Zr alloys, indicating that it is not strongly inhibited by Zr in the alloys with a low β-stabilizer content. The influence of Zr on the deformation behaviours of the alloys is weak because Zr and Ti are of the same family in the periodic table and twinning is also a deformation mechanism of β-Zr [38].

The strengths of Ti−12Nb−2Fe−(2, 4, 6, 8)Zr alloys are obviously greater than those of Ti−(14−24)Nb−2Fe alloys [20], indicating that Zr shows a much greater solid-solution strengthening effect than Nb. Ti−12Nb−2Fe−8Zr consists of single β phase, but the α'' phase appears in Ti−18Nb−8Zr after solution treatment [39]. This indicates that compared to 6 at.% Nb addition, 2 at.% Fe addition exhibits greater ability to stabilize the β phase and inhibit the α'' phase transformation during quenching. The $TiFe_2$ intermetallic compound is not observed in all the alloys owing to the small amount of Fe, but Ti−12Nb−2Fe−8Zr shows much higher $\sigma_{0.2}$ and σ_b than Ti−18Nb−8Zr [39], suggesting that Fe also

shows a much greater solid-solution strengthening effect than Nb.

A low elastic modulus is usually obtained in Ti alloy with single metastable β phase, and Zr is beneficial to reducing the elastic modulus of Ti alloys. The solid-solution strengthening effect of Fe and Zr increases the strength of the alloys, and the appearance of twinning during deformation is beneficial to increasing the ductility and work hardening. The synergistic effect of the strengthening mechanism and deformation mechanism makes the alloys exhibit high strength and high plasticity. Ti−12Nb−2Fe−(8, 10)Zr alloys with the metastable β phase both show a elastic modulus lower than 65 GPa, which is close to those of Ti−29Nb−13Zr−4.6Zr (wt.%), Ti−24Nb−4Zr−8Sn (wt.%), and Ti−35Nb−7Zr−5Ta (wt.%), and lower than those of cp-Ti, Ti−6Al−4V (wt.%), Ti−15Mo (wt.%), and Ti−13Nb−13Zr (wt.%) [40]. Moreover, the addition of Fe and Zr and the occurrence of twinning make Ti−12Nb−2Fe−8Zr and Ti−12Nb−2Fe−10Zr exhibit tensile strengths of 750 MPa and 780 MPa and elongations of 34% and 24%, respectively. Therefore, the Ti−12Nb−2Fe−(8, 10)Zr alloys show great potential for implant materials.

5 Conclusions

(1) The increase in Zr content inhibits the ω and α'' transformations in Ti−12Nb−2Fe−(2, 4, 6, 8, 10)Zr during quenching. The ω phase is found in Ti−12Nb−2Fe−2Zr, and the α'' phase is found in Ti−12Nb−2Fe−6Zr. Furthermore, Ti−12Nb−2Fe−(8, 10)Zr alloys consist of single β phase.

(2) The deformation mode is only slightly changed by Zr addition. Twinning is observed in all the deformed alloys and reveals twinning-induced plasticity. All the alloys exhibit obvious work hardening during plastic deformation. The solid-solution strengthening of Zr can almost counteract the strength reduction caused by the disappearance of ω-phase precipitation strengthening.

(3) Low elastic moduli are obtained in Ti−12Nb−2Fe−(8, 10)Zr with single metastable β phase. Under the joint effect of solid-solution strengthening and twinning-induced plasticity, Ti−12Nb−2Fe−(8, 10)Zr alloys show high strengths and good plasticity and are suitable for using as biomedical implants.

Acknowledgments

This work was financially supported by the Natural Science Foundation of Shanghai, China (No. 15ZR1428400), Shanghai Engineering Research Center of High-Performance Medical Device Materials, China (No. 20DZ2255500), the Project of Creation of Life Innovation Materials for Interdisciplinary and International Researcher Development, Tohoku University, sponsored by Ministry, Education, Culture, Sports, Science and Technology, Japan, and the Grant-in Aid for Scientific Research (C) (No. 20K05139) from JSPS (Japan Society for the Promotion of Science), Tokyo, Japan.

References

[1] HAO Yu-lin, LI Shu-jun, YANG Rui. Biomedical titanium alloys and their additive manufacturing [J]. Rare Metals, 2016, 35(9): 661−671.

[2] HASHMI M L, WADOOD A. Microstructural, mechanical and shape memory characterizations of Ti−Mo−Sn alloys [J]. Transactions of Nonferrous Metals Society of China, 2020, 30(3): 688−700.

[3] ZHANG Lai-chang, CHEN Liang-yu. A review on biomedical titanium alloys: Recent progress and prospect [J]. Advanced Engineering Materials, 2019, 21(4): 1801215−1801243.

[4] LIU Yong, TANG Han-chun, HUANG Qian-li, ZHAO Da-peng, HE Jun-yang, CAO Yuan-kui, SONG Min, LIU Bin, OUYANG Si-hui. Strong-yet-ductile Ti−Zr alloys through high concentration of oxygen strengthening [J]. Transactions of Nonferrous Metals Society of China, 2020, 30(9): 2449−2458.

[5] HAGHIGHI S E, LU H B, JIAN G Y, CAO G H, HABIBI D, ZHANG L C. Effect of α'' martensite on the microstructure and mechanical properties of beta-type Ti−Fe−Ta alloys [J]. Materials & Design, 2015, 76: 47−54.

[6] NIINOMI M, NAKAI M, HIEDA J. Development of new metallic alloys for biomedical applications [J]. Acta Biomaterialia, 2012, 8: 3888−3903.

[7] HAN Li-ying, WANG Cun-shan. Microstructure and properties of $Ti_{64.51}Fe_{26.40}Zr_{5.86}Sn_{2.93}Y_{0.30}$ biomedical alloy fabricated by laser additive manufacturing [J]. Transactions of Nonferrous Metals Society of China, 2020, 30(12): 3274−3286.

[8] MIAO Jing-lei, LIU Jue, WANG Hui-feng, YANG Hai-lin, RUAN Jian-ming. Preparation of porous Ta−10%Nb alloy scaffold and its in vitro biocompatibility evaluation using MC3T3-E1 cells [J]. Transactions of Nonferrous Metals Society of China, 2018, 28(10): 2053−2061.

[9] LIU X Y, CHU P K, DING C X. Surface modification of titanium, titanium alloys, and related materials for biomedical applications [J]. Materials Science and Engineering R, 2004, 47: 49−121.

[10] KIM J I, KIM H Y, INAMURA T, HOSODA H, MIYAZAKI

S. Shape memory characteristics of Ti−22Nb−(2−8)Zr (at.%) biomedical alloys [J]. Materials Science and Engineering A, 2005, 403: 334−339.

[11] SUN Hong, YU Li-ming, LIU Yong-chang., ZHANG Li-ye, LIU Chen-xi, LI Hui-jun, WU Jie-feng. Effect of heat treatment processing on microstructure and tensile properties of Ti−6Al−4V−10Nb alloy [J]. Transactions of Nonferrous Metals Society of China, 2019, 29(1): 59−66.

[12] MORAES P E L, CONTIERI R J, LOPES E S N, ROBIN A, CARAM R. Effects of Sn addition on the microstructure, mechanical properties and corrosion behavior of Ti−Nb−Sn alloys [J]. Materials Characterization, 2014, 96: 273−281.

[13] HAO Y L, LI S J, SUN S Y, YANG R. Effect of Zr and Sn on Young's modulus and superelasticity of Ti−Nb-based alloys [J]. Materials Science and Engineering A, 2006, 441(1/2): 112−118.

[14] KURODA D, NIINOMI M, MORINAGA M, KATO Y, YASHIRO T. Design and mechanical properties of new β type titanium alloys for implant materials [J]. Materials Science and Engineering A, 1998, 243: 244−249.

[15] ZHOU Li-bo, YUAN Tie-chui, LI Rui-di, TANG Jian-zhong, WANG Min-bo. Anisotropic mechanical behavior of biomedical Ti−13Nb−13Zr alloy manufactured by selective laser melting [J]. Journal of Alloys and Compounds, 2018, 762: 289−300.

[16] HENDRICKSON M, MANTRI S A, REN Y, ALAM T, SONI V, GWALANI B, STYLES M, CHOUDHURI D, BANERJEE R. The evolution of microstructure and microhardness in a biomedical Ti−35Nb−7Zr−5Ta alloy [J]. Journal of Materials Science, 2017, 52: 3062−3073.

[17] LI Qiang, NIINOMI M, NAKAI M, CUI Zhen-duo, ZHU Sheng-li, YANG Xian-jin. Effect of Zr on super-elasticity and mechanical properties of Ti−24at.%Nb−(0, 2, 4)at.% Zr alloy subjected to aging treatment [J]. Materials Science and Engineering A, 2012, 536: 197−206.

[18] LOPES É S N, SALVADOR C A F, ANDRADE D R, CREMASCO A, CAMPO K N, CARAM R. Microstructure, mechanical properties, and electrochemical behavior of Ti−Nb−Fe alloys applied as biomaterials [J]. Metallurgical and Materials Transactions A, 2016, 47(6): 3213−3226.

[19] QI Peng, LI Bo-long, WANG Tong-bo, ZHOU Lian, NIE Zuo-ren. Microstructure and properties of a novel ternary Ti−6Zr−xFe alloy for biomedical applications [J]. Journal of Alloys and Compounds, 2021, 854: 157119−157126.

[20] LI Qiang, MIAO Pu, LI Jun-jie, HE Mei-feng, NAKAI M, NIINOMI M, CHIBA A, NAKANO T, LIU Xu-yan, ZHOU Kai, PAN Deng. Effect of Nb content on microstructures and mechanical properties of Ti−xNb−2Fe alloys [J]. Journal of Materials Engineering and Performance, 2019, 28(9): 5501−5508.

[21] ENDOH K, TAHARA M, INAMURA T, HOSODA H. Effect of Sn and Zr addition on the martensitic transformation behavior of Ti−Mo shape memory alloys [J]. Journal of Alloys and Compounds, 2017, 695: 76−82.

[22] ZHOU Yu, LI Yu-xuan, YANG Xian-jin, CUI Zhen-duo, ZHU Sheng-li. Influence of Zr content on phase transformation, microstructure and mechanical properties of $Ti_{75-x}Nb_{25}Zr_x$ (x=0−6) alloys [J]. Journal of Alloys and Compounds, 2009, 486(1/2): 628−632.

[23] LI Qiang, MA Guang-hao, LI Jun-jie, NIINOMI M, NAKAI M, KOIZUMI Y, WEI Dai-xiu, KAKESHITA T, NAKANO T, CHIBA A, LIU Xu-yan, ZHOU Kai, PAN Deng. Development of low-Young's modulus Ti−Nb-based alloys with Cr addition [J]. Journal of Materials Science, 2019, 54(11): 8675−8683.

[24] HAO Y L, YANG R, NIINOMI M, KURODA D, FUKUNAGA K, ZHOU Y L, YANG R, SUZUKI A. Young's modulus and mechanical properties of Ti−29Nb−13Ta−4.6Zr in relation to α'' martensite [J]. Metallurgical and Materials Transactions A, 2002, 33: 3137−3144.

[25] WANG Qing, DONG Chuang, LIAW P K. Structural stabilities of β-Ti alloys studied using a new Mo equivalent derived from [β/(α+β)] phase-boundary slopes [J]. Metallurgical and Materials Transactions A, 2015, 46: 3440−3447.

[26] KOLLI R P, JOOST W J, ANKEM S. Phase stability and stress-induced transformations in beta titanium alloys [J]. JOM, 2015, 67(6): 1273−1280.

[27] CASTANY P, YANG Y, BERTRAND E, GLORIANT T. Reversion of a parent $\{130\}\langle 110\rangle_{\alpha''}$ martensitic twinning system at the origin of $\{332\}\langle 113\rangle_{\beta}$ twins observed in metastable β titanium alloys [J]. Physical Review Letters, 2016, 117: 245501−245507.

[28] ZENER C, HOLLOMON J H. Effect of strain rate upon plastic flow of steel [J]. Journal of Applied Physics, 1944, 15(1): 22−32.

[29] LIMBADRI K, SINGH S K, SATYANARAYANA K, SINGH A K, RAM A M, RAVINDRAN M, KRISHNA K V M, REDDY M C, SURESH K. Orientation-dependent tensile flow behavior of Zircaloy-4 at room temperature [J]. Metallography, Microstructure, and Analysis, 2018, 7(4): 421−433.

[30] MARTELEUR M, SUN F, GLORIANT T, VERMAUT P, JACQUES P J, PRIMA F. On the design of new β-metastable titanium alloys with improved work hardening rate thanks to simultaneous TRIP and TWIP effects [J]. Scripta Materialia, 2012, 66: 749−752.

[31] BROZEK C, SUN F, VERMAUT P, MILLET Y, LENAIN A, EMBURY D, JACQUES P J, PRIMA F. A β-titanium alloy with extra high strain-hardening rate: Design and mechanical properties [J]. Scripta Materialia, 2016, 114: 60−64.

[32] MATLAKHOVA L A, MATLAKHOV A N, MONTEIRO S N, FEDOTOV S G, GONCHARENKO B A. Properties and structural characteristics of Ti−Nb−Al alloys [J]. Materials Science and Engineering A, 2005, 393: 320−326.

[33] ZHOU Ying-long, NIINOMI M, AKAHORI T. Effects of Ta content on Young's modulus and tensile properties of binary Ti−Ta alloys for biomedical applications [J]. Materials Science and Engineering A, 2004, 371: 283−290.

[34] SAITO T, FURUTA T, HWANG J H, KURAMOTO S, NISHINO K, SUZUKI N, CHEN R, YAMADA A, ITO K, SENO Y, NONAKA T, IKEHATA H, NAGASAKO N, IWAMOTO C, IKUHARA Y, SAKUMA T. Multifunctional alloys obtained via a dislocation-free plastic deformation mechanism [J]. Science, 2003, 300: 464−467.

[35] TANE M, HAGIHARA K, UEDA M, NAKANO T, OKUDA Y. Elastic-modulus enhancement during room-temperature aging and its suppression in metastable Ti−Nb-based alloys

with low body-centered cubic phase stability [J]. Acta Materialia, 2016, 102: 373−384.

[36] ZHAO X F, NIINOMI M, NAKAI M, HIEDA J. Beta type Ti−Mo alloys with changeable Young's modulus for spinal fixation applications [J]. Acta Biomaterialia, 2012, 8: 1990−1997.

[37] LI Qiang, CHENG Chao, LI Jun-jie, ZHANG Ke, ZHOU Kai, NAKAI M, NIINOMI M, YAMANAKA K, WEI Dai-xiu, CHIBA A, NAKANO T. Low Young's modulus and high strength obtained in Ti−Nb−Zr−Cr alloys by optimizing Zr content [J]. Journal of Materials Engineering and Performance, 2020, 29(5): 2871−2878.

[38] SKVORTSOV A I, SKVORTSOV A A. Amplitude dependence of internal friction of zirconium and alloys Zr−8%Nb and Zr−20%Nb [J]. Physics of Metals and Metallography, 2018, 119: 634−642.

[39] ZHANG Jin-yong, SUN Fan, HAO Yu-lin, GOZDECKI N, LEBRUN E, VERMAUT P, PORTIER R, GLORIANT T, LAHEURTE P, PRIMA F. Influence of equiatomic Zr/Nb substitution on superelastic behavior of Ti−Nb−Zr alloy [J]. Materials Science and Engineering A, 2013, 563: 78−85.

[40] ZHANG Lai-chang, CHEN Liang-yu, WANG Li-qiang. Surface modification of titanium and titanium alloys: Technologies, developments, and future interests [J]. Advanced Engineering Materials, 2020, 22(5): 1901258−1901294.

高强度和低弹性模量 Ti−Nb−Fe−Zr 合金的显微组织和力学性能

李 强[1]，黄 奇[1]，李俊杰[2]，何黔峰[1]，Masaaki NAKAI[3]，张 柯[4]，
Mitsuo NIINOMI[1,5,6,7]，Kenta YAMANAKA[5]，Akihiko CHIBA[5]，Takayoshi NAKANO[6]

1. 上海理工大学 机械工程学院，上海 200093；
2. 中国科学院 新疆理化技术研究所 特殊环境功能材料与器件重点实验室，乌鲁木齐 830011；
3. Division of Mechanical Engineering, Faculty of Science and Engineering, Kindai University, 3-4-1 Kowakae, Higashiosaka, Osaka 577-8502, Japan;
4. 上海理工大学 材料科学与工程学院，上海 200093；
5. Institute for Materials Research, Tohoku University, 2-1-1 Katahira, Aoba-ku, Sendai 980-8577, Japan;
6. Division of Materials and Manufacturing Science, Graduate School of Engineering, Osaka University, 2-1 Yamada-Oka, Suita, Osaka 565-0871, Japan;
7. Department of Materials Science and Engineering, Graduate School of Science and Technology, Meijo University, 1-501 Shiogamaguchi, Tempaku-ku, Nagoya 468-8502, Japan

摘 要：将 Zr 添加到 Ti−Nb−Fe 合金中开发生物医用低模量、高强度 β 钛合金。采用电弧熔炼法制备 Ti−12Nb−2Fe−(2, 4, 6, 8, 10)Zr (摩尔分数，%)铸锭，随后对其进行均匀化、冷轧和固溶处理。通过光学显微镜、X 射线衍射和透射电子显微镜等技术分析合金的物相和显微组织。采用拉伸试验测定力学性能。结果表明，Zr 和 Fe 在合金中具有显著的固溶强化效果，因此，所有合金的屈服强度和抗拉强度分别高于 510 MPa 和 730 MPa。Zr 对变形机制的影响较小，孪晶出现在所有变形合金中，且对强度和塑性有益。具有亚稳 β 相的 Ti−12Nb−2Fe−(8, 10)Zr 合金表现出低弹性模量、高抗拉强度和良好的塑性，是生物医学植入物的合适候选材料。

关键词：医用钛合金；力学性能；固溶强化；加工硬化；孪晶诱导塑性

(Edited by Wei-ping CHEN)